remote sensing

MDPI

Article

Characterizing Spatiotemporal Variations in the Urban Thermal Environment Related to Land Cover Changes in Karachi, Pakistan, from 2000 to 2020

Muhammad Fahad Baqa [1,2,3], Linlin Lu [1,3,*], Fang Chen [1,3], Syed Nawaz-ul-Huda [4], Luyang Pan [1,3], Aqil Tariq [5], Salman Qureshi [6], Bin Li [1,3] and Qingting Li [7]

1 Key Laboratory of Digital Earth Science, Aerospace Information Research Institute, Chinese Academy of Sciences, Beijing 100094, China; 2252293808@mails.ucas.edu.cn (M.F.B.); chenfang@radi.ac.cn (F.C.); panluyangyyy@163.com (L.P.); libin01@radi.ac.cn (B.L.)
2 University of Chinese Academy of Science, Beijing 100049, China
3 International Research Center of Big Data for Sustainable Development Goals, Beijing 100094, China
4 Dawn GIS, Geospatial Statistical Research & Analysis Division, Karachi 75300, Pakistan; nawaz_huda@hotmail.com
5 State Key Laboratory of Information Engineering in Surveying, Mapping and Remote Sensing (LIESMARS), Wuhan University, Wuhan 430079, China; aqiltariq@whu.edu.cn
6 Institute of Geography, Humboldt University of Berlin, 12489 Berlin, Germany; salman.qureshi@geo.hu-berlin.de
7 Airborne Remote Sensing Center, Aerospace Information Research Institute, Chinese Academy of Sciences, Beijing 100094, China; liqt@radi.ac.cn
* Correspondence: lull@radi.ac.cn

Abstract: Understanding the spatiotemporal patterns of urban heat islands and the factors that influence this phenomenon can help to alleviate the heat stress exacerbated by urban warming and strengthen heat-related urban resilience, thereby contributing to the achievement of the United Nations Sustainable Development Goals. The association between surface urban heat island (SUHI) effects and land use/land cover features has been studied extensively, but the situation in tropical cities is not well-understood due to the lack of consistent data. This study aimed to explore land use/land cover (LULC) changes and their impact on the urban thermal environment in a tropical megacity—Karachi, Pakistan. Land cover maps were produced, and the land surface temperature (LST) was estimated using Landsat images from five different years over the period 2000–2020. The surface urban heat island intensity (SUHII) was then quantified based on the LST data. Statistical analyses, including geographically weighted regression (GWR) and correlation analyses, were performed in order to analyze the relationship between the land cover composition and LST. The results indicated that the built-up area of Karachi increased from 97.6 km^2 to 325.33 km^2 during the period 2000–2020. Among the different land cover types, the areas classified as built-up or bare land exhibited the highest LST, and a change from vegetation to bare land led to an increase in LST. The correlation analysis indicated that the correlation coefficients between the normalized difference built-up index (NDBI) and LST ranged from 0.14 to 0.18 between 2000 and 2020 and that NDBI plays a dominant role in influencing the LST. The GWR analysis revealed the spatial variation in the association between the land cover composition and the SUHII. Parks with large areas of medium- and high-density vegetation play a significant role in regulating the thermal environment, whereas the scattered vegetation patches in the urban core do not have a significant relationship with the LST. These findings can be used to inform adaptive land use planning that aims to mitigate the effects of the UHI and aid efforts to achieve sustainable urban growth.

Keywords: surface urban heat island; land surface temperature; megacity; sustainable development goals; Karachi

Citation: Baqa, M.F.; Lu, L.; Chen, F.; Nawaz-ul-Huda, S.; Pan, L.; Tariq, A.; Qureshi, S.; Li, B.; Li, Q. Characterizing Spatiotemporal Variations in the Urban Thermal Environment Related to Land Cover Changes in Karachi, Pakistan, from 2000 to 2020. *Remote Sens.* **2022**, *14*, 2164. https://doi.org/10.3390/rs14092164

Academic Editors: Paul Osmond and Carlos Bartesaghi Koc

Received: 30 March 2022
Accepted: 26 April 2022
Published: 30 April 2022

1. Introduction

Urbanization refers to the growth and modernization of cities and the migration of people from rural to urban areas. Currently, cities contain more than half of the world's population [1], with the last few decades having seen a significant increase in urbanization across the globe. The proportion of the global population living in urban areas is predicted to rise to 68% by 2050 from its present value of 55%, and nearly 90% of this growth will take place in Asia and Africa [2]. The 11th goal of the 2030 Agenda for Sustainable Development adopted by the United Nations member states in 2015 targets the crucial role of urban settlements in fostering sustainable development and focuses on developing inclusive, sustainable, and resilient urban environments [3]. Urbanization has led to a rapid increase in the geographic extent of urban areas. This has a major effect on the local environment's energy balance and results in the urban heat island (UHI) effect, which can be defined as a situation wherein the surface temperature in cities is higher than that of the surrounding areas [4–6]. This local difference in temperature negatively impacts both people and the environment, because it can decrease the air quality, lead to increased energy consumption, and affect people's health [7,8]. The projected global temperature increase combined with the increasing UHI effect will make developing countries more susceptible to heat-related deaths and illnesses. Understanding the spatiotemporal patterns in urban heat islands and the factors that influence this effect can help to mitigate the negative impacts of urban warming, improve urban resilience, and contribute to the achievement of the sustainable development goals in urban settlements.

Urbanization-induced land use and land cover (LULC) change has drastically increased as a result of the rapid economic development and growing population in recent decades [9]. Since LULC change is most common in developing countries in the central parts of individual cities, investigating land cover change and the accompanying environmental impacts in developing countries is critical [10]. Hassan et al. [11] analyzed land cover change and its influence on the surface urban heat island intensity (SUHII) in seven Asian megacities—namely, Kabul, Dhaka, Thimphu, Delhi, Kathmandu, Colombo, and Karachi. The LULC in each city was classified using a machine learning classifier and Landsat data and was linked to changes in the thermal environment [11]. Kikon et al. [12] assessed temporal changes in rising trends of UHI in Noida City, India, using Landsat data and grid-level analysis, and compared them with the LULC change pattern. Arshad et al. [13] evaluated the impacts of LULC changes on the surface urban heat island and revealed that the reduction of green space in old city areas and transition zones caused high LST and warming in Lahore, Pakistan. The loss of vegetative cover during the urbanization process and its correlation with the increase in LST have also been reported in Islamabad [14].

As remote sensing sensors have developed, thermal infrared remote sensing has become crucial to the retrieval of LSTs [15,16] and the investigation of surface urban heat island (SUHI) effects [17–19]. The UHI phenomenon has been described in several Asian countries [20–22]. A time series analysis was performed to analyze the intensity of the urban heat island in eight Asian megacities, including Karachi, from 1992 to 2012 [23]. In particular, the combination of multispectral data with thermal infrared imagery acquired by the Landsat TM, ETM+, OLI, and TIRS sensors improved our ability to obtain LSTs and land cover change information while simultaneously using the same datasets. As compared with satellite remote sensing data, such as MODIS and ASTER, a key benefit of Landsat data is the long-term temporal range (Landsat-4 and 5 TM data are available from 1980 onwards) [24]. Remote sensing spectral indices can quantitatively represent the land cover composition and were correlated with the LST in several studies [25,26]. Zhou et al. [27] analyzed the impact of land cover composition on the thermal environment in Washington DC, USA. The correlation between LST and the normalized difference vegetation index (NDVI) and the normalized difference built-up index (NDBI) suggest that they exert a negative and positive effect on LST in tropical and subtropical regions, respectively [18,21].

Karachi is one of Pakistan's fastest-growing and largest megacities and has a high population density. Together with the rapid urban development that has occurred in recent decades, the thermal environment of the city has deteriorated rapidly. However, as a result of the spatial scarcity and the inconsistent distribution of existing meteorological stations, especially in developing countries such as Pakistan, accurate estimations of changes in SUHII remain challenging. Thus, there are only a few previous studies that have focused on the thermal environment of Karachi. The changes in SUHI in Karachi and its relationship with rapid urbanization and LULC were analyzed based on day and nighttime LST data from MODIS and Landsat images in 2009 and 2017 [28]. Hassan et al. [11] conducted a comparative study to examine the changes in the thermal environment in seven South Asian megacities from 2000 to 2019 using yearly average LST from MODIS data with a 1-km spatial resolution. A comparative study was conducted to detect the urbanization patterns of four rapidly developing lowland South Asian cities, including Karachi, in 2019 [29]. Despite these efforts, multitemporal satellite remote sensing data have been insufficiently employed, and our knowledge on the long-term evolution of SUHI and concurrent LULC changes in Karachi is still lacking.

In June 2015, a heatwave struck Karachi and killed more than 1000 people [30]. It is necessary to comprehensively investigate the spatiotemporal changes of the urban thermal environment in the Karachi metropolitan region. The reliability on support vector machines for remote sensing image classification and the LULC change analysis has been demonstrated in various studies [31–33]. In this study, the LULC was classified using the support vector machine method, and the LST datasets were derived from Landsat images in Karachi. The relationships between these datasets were then explored through a bivariate correlation analysis and geographically weighted regression (GWR) statistical analysis. The study's specific objectives were: (1) to analyze the LULC changes, (2) to explore the spatial and temporal variations in the urban thermal environment with a primary focus on hotspots, and (3) to explore the relationship between the LST and LULC patterns using the GWR model in Karachi.

2. Materials and Methods

2.1. Study Area

Karachi, Pakistan's largest and most densely populated city, is the provincial capital of Sindh Province. It is the country's primary seaport, industrial center, and financial hub. The Karachi urban agglomeration, which covers 3527 km^2, is located on the Arabian Sea coastline between 24.45°N and 25.15°N and between 66.37°E and 67.37°E (Figure 1). The Lyari and Malir Rivers flow through the city on their way to the Arabian Sea. Administratively, the city is divided into seven districts and 31 subdivisions [34]. Karachi's urban population has grown from 9.45 million in 1998 to 14.91 million in 2017. According to the United Nations' estimates [35], the city's population will reach more than 20 million by 2025. The rapid rate of urbanization during the last three decades has had negative consequences for the environment, specifically in relation to the UHI, air pollution, and energy consumption, as a result of the lack of urban expansion planning and insufficient essential public infrastructure and facilities [36].

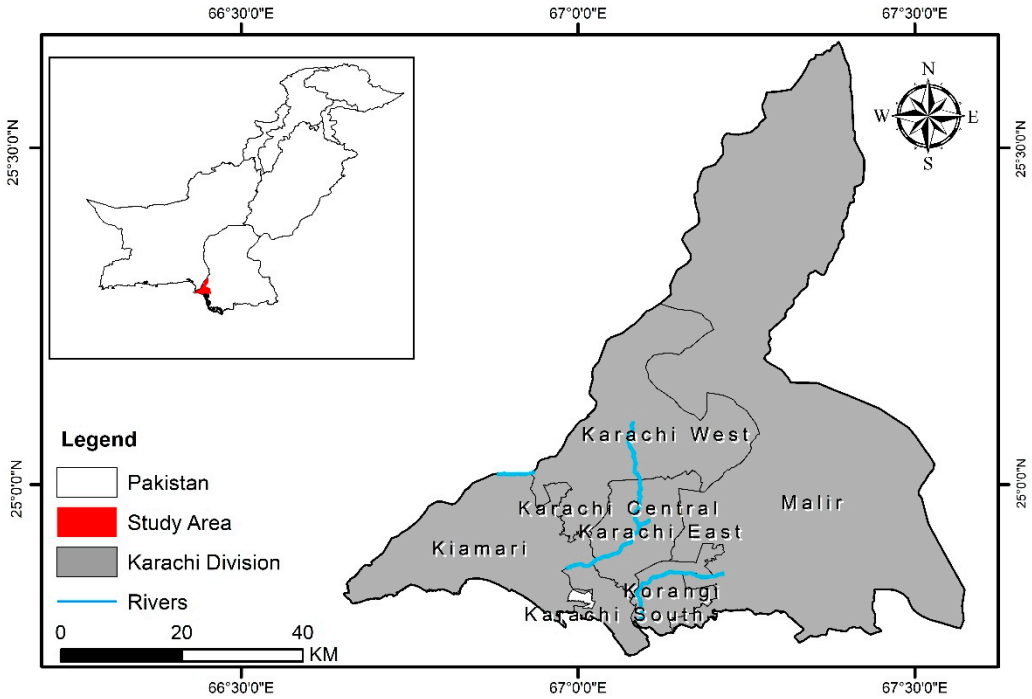

Figure 1. The geographical location of the study area.

2.2. Datasets

Eleven Landsat images acquired between 2000 and 2020 were utilized to map the land use/land cover changes and the urban thermal environment with 5-year intervals (Table 1). The images were acquired by Landsat 5 TM, 7 ETM+, and 8 OLI/TIRS. Landsat data consisted of collection 2, level 2 data obtained from the United States Geological Survey (https://earthexplorer.usgs.gov, accessed on 12 August 2021). The entire study area covered three Landsat tiles (152_042, 152_043, and 153_043). The land surface temperature could be determined from thermal infrared (TIR) measurements of satellite sensors. However, the TIR measurements are very sensitive to cloud contamination, which precludes an accurate determination of the LST [37]. In addition, precipitation can cause large variations in the surface emissivity. Thus, seasonal differences can influence remote sensing image availability (increased cloud cover) and accuracy in LST measurements. In order to reduce the uncertainties of LST determination, satellite images with a minimum amount of cloud coverage (<10%) corresponding to the driest months (September–November) were collected in our study [38,39]. Table 1 lists the ten Landsat scenes that were used for LST retrieval in this study.

Table 1. Details of the Landsat imagery used.

Year	Date	Satellite and Sensor	Spatial Resolution (m)
2000	26 October 2000 1 October 2000	Landsat5 TM Landsat5 TM	30 30
2005	16 October 2005 7 October 2006	Landsat7 ETM+ Landsat5 TM	30 30
2010	7 November 2010 21 October 2010	Landsat5 TM Landsat7 ETM+	30 30
2015	5 November 2015 12 November 2015	Landsat8 OLI Landsat8 OLI	30 30
2020	1 October 2020 24 October 2020	Landsat8 OLI Landsat8 OLI	30 30

3. Methods

In our study, the entire data processing and analysis workflow included several steps. First of all, the land use/land cover types were classified, and the land surface temperature was retrieved from the Landsat images. Thereafter, the intensity of the SUHI was quantified using the LST and land cover classification data. Finally, the relationship between the LST and land cover was explored. Figure 2 is an overview of the data processing workflow in this study.

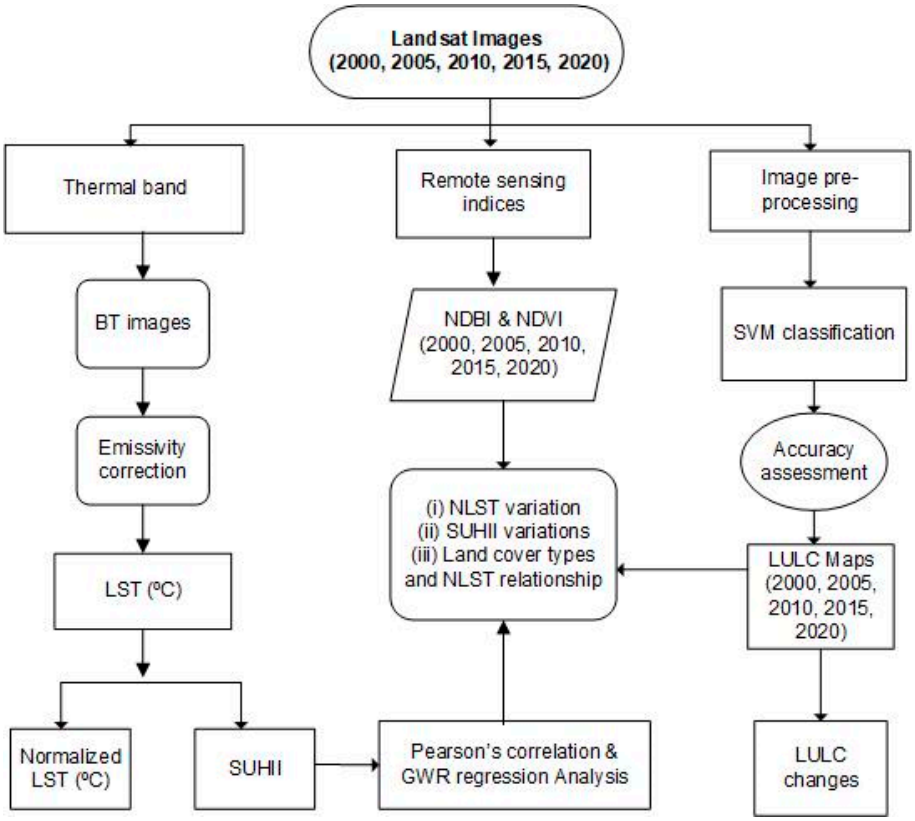

Figure 2. Data processing workflow.

3.1. Land Use/Land Cover Classification

The support vector machine (SVM) approach has been widely used for LULC classification with multisource remote sensing data and has exhibited its capacity to obtain accurate results [31–33]. The SVM classifier with a radial basis function kernel, and a penalty hyperparameter of 100 was used here to classify the land cover into four broad types: built-up area, bare land, water bodies, and vegetation. As one of the most widely used kernels, the radial basis function kernel is in the form of a Gaussian function and can obtain optimal results for nonlinear data. For each LULC class, around 150 samples were collected to ensure sufficient representation [40]. High-resolution satellite images in Google Earth and pan-sharpened versions of Landsat data were used to gather ground truth information [41]. The LULC classes and their descriptions are shown in Table 2, together with the number of training and testing pixels used during the SVM classification.

Quantitative metrics were used to assess the accuracy of each classified image. Ground truth regions for classification accuracy assessment were created using ancillary land cover change data from topographical maps and urban LULC maps acquired from the Survey department of Pakistan and Karachi Municipal Corporation [34]. The ground truth data were interpreted based on their spectral characteristics and a literature review with additional ancillary information.

Table 2. LULC classification scheme and class descriptions.

LULC Class	Description	No. of Training Pixels	No. of Testing Pixels
Water bodies	Rivers, permanent open water, lakes, ponds, and reservoirs	60	120
Built-up area	Residential areas, land used for commerce and services, industry, transportation, and roads	150	240
Vegetation	Agricultural areas, crops, fallow land and vegetation, and scrub	150	240
Bare land	Exposed soils, landfill sites, areas of active excavation, and open bare land	150	240

3.2. Land Surface Temperature Retrieval

The land surface temperature was retrieved using a radiative transfer equation (RTE) [41]. Normalized LST values can provide objective information about the spatial distribution of the LST values extracted from satellite images obtained under a variety of atmospheric, temporal, and lighting conditions [42]. The LST values were standardized using Equation (1) to ensure the information extracted from satellite imagery captured over multiple years was comparable.

$$\mathrm{NLST} = (\mathrm{LST_i} - \mathrm{LST_{min}})/(\mathrm{LST_{max}} - \mathrm{LST_{min}}), \quad (1)$$

where NLST is the normalized LST, $\mathrm{LST_i}$ is the pixel i initial LST, and $\mathrm{LST_{min}}$ and $\mathrm{LST_{max}}$ are the minimum and maximum LST in a given scene, respectively.

3.3. Calculation of the Surface Urban Heat Island Intensity

The most popular method for modeling the effects of urban growth and land cover change on the SUHII is to calculate the temperature differences between urban and rural areas. Since the definitions of urban and rural areas vary greatly from country to country, there is no standardized method to distinguish urban areas and rural areas [4]. Under the framework of the local climatic zone (LCZ), the SUHII was measured as the differential LST between built-up and green space areas [43]. As the LST within the areas of green space varied, an average LST was used as a reference for mapping SUHII. In this study, the SUHI intensity was measured as the difference in LSTs between built-up areas and areas of green space [44]. The SUHII was calculated for each built-up area pixel using Equation (2):

$$\mathrm{SUHII}_i = T_{bui} - \overline{T}_{gs}, \quad (2)$$

where T_{bui} is the land surface temperature at pixel i, and $\overline{T}_{gs}$, is the mean land surface temperature of the green space pixels. The green space pixels of the study area were determined using the LULC classification map. The SUHII for the whole study area was calculated using Equation (3):

$$\mathrm{SUHII} = \frac{1}{n} \sum_{i=1}^{n} \mathrm{SUHII}_i, \quad (3)$$

where SUHII_i is the surface urban heat island intensity at pixel i, and n is the total number of built-up pixels.

Following Reference [41], we classified the areas in the SUHII maps into five classes: no SUHII (SUHII < 0.00), low SUHII (0.00–2.00), moderate SUHII (2.00–4.00), high SUHII (4.00–6.00), and very high or extreme SUHII (>6.00).

3.4. Statistical Analysis

According to a systematic review [45], the majority of previous studies (>68%) tended to utilize global-based analysis to quantify the relationship between spatial variables and UHI variables. The ordinary least squares (OLS) regression, which assumes constant relationships over spaces between the independent and dependent variables, is the most commonly used approach. On the regional scale, however, the SUHI effect may be context-sensitive and vary considerably over time and location [46]. In this study, both bivariate

correlation analysis and geographically weighted regression (GWR) were used to quantify the relationships between the LST and the land cover composition [47]. Pearson's correlation coefficient was used to quantify the correlation between these two variables. We selected 1000 random samples to conduct a correlation analysis between the NLST, NDVI, and NDBI.

Geographically weighted regression is a technique in which the spatial heterogeneity of the relationships between the independent variables and the dependent variable can be captured [48,49]. The following formula was used for GWR:

$$y_i = \beta_0(u_i, v_i) + \sum_k \beta_k(u_i, v_i)x_{ik} + \varepsilon_i, \quad (4)$$

where (u_i, v_i) indicates the spatial coordinates of observation i, β_0 and β_k are the estimated parameters, and ε_i denotes the random error in terms of observation i. Each observation is assigned a weight based on the distance decay function. The weighting of an observation is not constant but is a function of the geographical location. Larger weights are assigned to observations closer to point i [50]. The inverse distance weighting has been adopted in different environmental studies [51–53]. In the GWR model, the relationships between the dependent and independent variables vary spatially [54]. The prediction performance of the GWR model can be improved by adjusting the regression coefficients according to the location. The kernel and bandwidth are the key parameters in the GWR model that affect the model accuracy. Herein, the adaptive Gaussian kernel was used because the 1000 sampling points were randomly distributed over an irregular study area. The model accuracy was evaluated using the coefficient of determination (R^2) and corrected Akaike Information Criterion (AICc). In this research, the GWR models were developed using ArcGIS 10.5 software.

4. Results

4.1. Land Use/Land Cover Change Analysis

The overall accuracies of the land cover maps that were produced ranged from 86.2% to 94.28% (Table 3). Details of individual maps of land cover changes are shown in Table 3. The maps show a continued expansion in the built-up area of Karachi over the period 2000–2020 (Figure 3). In the center of the city, the percentage cover of the built-up area was highest in 2000. Since then, the built-up area has gradually extended outward into the suburbs. Moreover, the amount of open bare land decreased significantly. The result reveals an interesting two-stage pattern in the land cover changes, i.e., first, the open bare land and vegetation were converted to open land and then into built-up areas. Thus, areas that were open bare land and vegetation in 2000 were converted to open land by 2010 and to built-up areas by 2015. By 2020, these built-up areas had become denser.

Figure 4 depicts the contribution of net changes in various LULC classes to changes in built-up areas. The Gadap, Bin Qasim, Murad Memon, Ibrahim Hyderi, Manghopir, Gulzar-i-Hijri Baldia, and Mauripur subdivisions experienced the largest increases in the built-up areas class. The smallest increases were in areas near the center of the city, such as The Garden, Saddar, Ferozabad, Harbor, Liaquatabad, SITE, Lyari, and Arambagh. Figure 4 shows that built-up area expansion primarily occurred due to the transformation of open bare land to built-up land in the northern and northeastern parts of the city. Vegetated areas were encroached upon by built-up areas in almost all parts of Karachi, except those near to the center. Moreover, in certain subdivisions, including The Garden, Saddar, Arambagh, Lyari, Civil Lines, Liaquatabad, and Harbor, there was only a slight increase in the area classed as built-up, because these were established CBD areas in which construction was restricted [56].

Table 3. Accuracy assessment of the classified maps.

Land Cover	2000		2005		2010		2015		2020	
	Prod.	User	Prod.	User	Prod.	User	Prod.	User	Prod.	User
Type	(%)	(%)	(%)	(%)	(%)	(%)	(%)	(%)	(%)	(%)
Built-up	97.5	100	75	93.75	95.12	97.29	90	97.43	87.5	87.5
Bare land	95	90.47	94.5	78	95.12	86.66	97.5	95.12	87.5	63.63
Vegetation	85	85	92.5	94.87	100	92.85	95	88.37	97.5	86.66
Water bodies	80	84.21	95	100	75	93.75	85	100	80	100
Overall accuracy (%)	90		89		92.14		94.28		86	
Kappa coefficient	0.8		0.85		0.8		0.92		0.86	

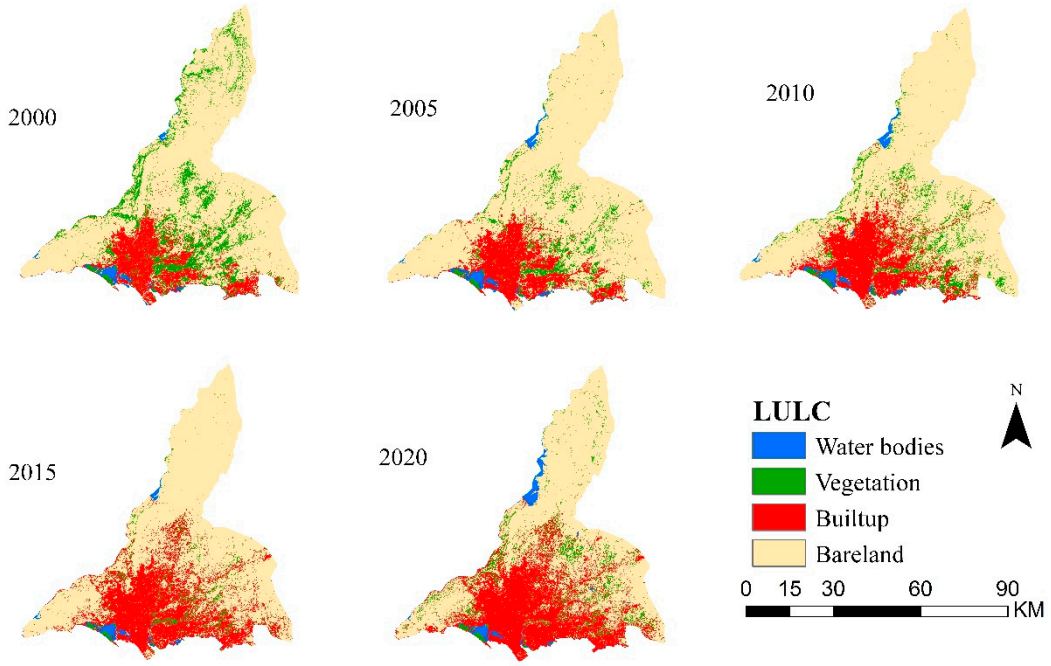

Figure 3. LULC maps of the study area estimated from Landsat data for the years 2000, 2005, 2010, 2015, and 2020.

Table 4 presents statistics for the LULC patterns in Karachi during the period 2000–2020. It can be seen that, between 2000 and 2020, the built-up area expanded by nearly 173%, from 440.19 km^2 to 765.52 km^2. Overall, the amount of vegetation cover and open bare land declined significantly over the same period. The amount of vegetation cover fluctuated, falling from 553.99 km^2 to 428.07 km^2 between 2000 and 2010 before increasing to 477.13 km^2 in 2015 and, finally, declining again to 378.13 km^2 in 2020. The amount of open bare land decreased from 2570.19 km^2 in 2000 to 2390.58 km^2 in 2020, whereas the area covered by water bodies increased from 43.54 km^2 to 86.53 km^2 between 2000 and 2020. A total of 179.61 km^2 of bare land and 175.86 km^2 of vegetation was converted into other land uses during this period (Figure 3). These LULC losses can be attributed to an increase in the urban area resulting from a high demand for residential space and space for business activities [55]. The open bare land and vegetation classes were those most affected by this rapid urbanization.

Table 4. LULC changes in Karachi during the period 2000–2020.

Land Cover Type	2000		2005		2010		2015		2020	
	Area (km^2)	Percentage	Area (km^2)	Percentage	Area (km^2)	Percentage	Area (km^2)	Percentage	Area (km^2)	Percentage
Built-up	440.19	12.20	537.79	14.91	606.49	16.80	680.62	18.79	765.52	21.14
Bare land	2570.19	71.24	2415.24	66.94	2512.99	69.63	2425.58	66.98	2390.58	66.02
Vegetation	553.99	15.35	465.01	12.89	428.07	11.86	477.13	13.18	378.13	10.44
Water bodies	43.54	1.21	58.80	1.63	61.59	1.71	38.14	1.05	86.53	2.39

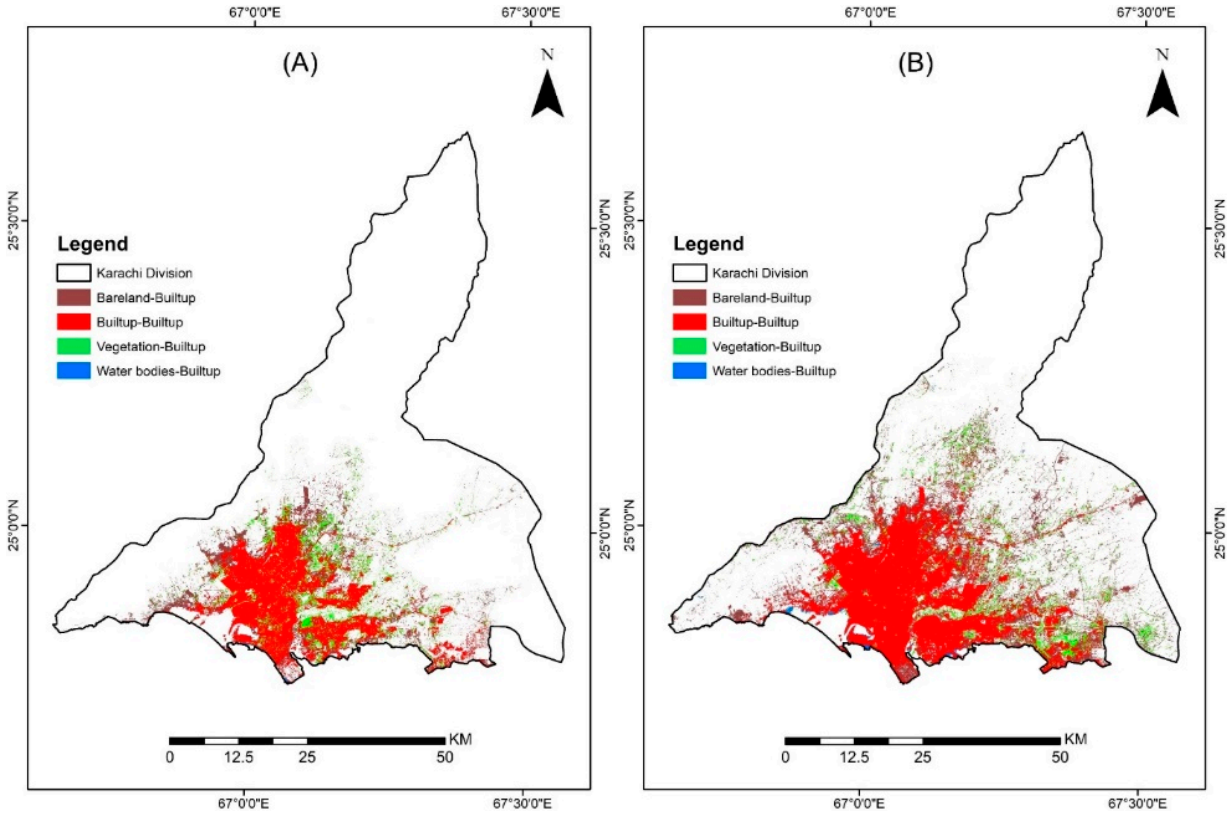

Figure 4. Details of the transition from other land use/land cover types to the built-up area class: (**A**) 2000–2010 and (**B**) 2010–2020.

4.2. Spatiotemporal Variations in the Urban Thermal Environment

4.2.1. Variations in the Normalized Land Surface Temperature

Figure 5 shows the classified NLST maps of the study area. Each map shows five classes of NLST—namely, very low temperature, low temperature, medium temperature, high temperature, and very high temperature. They were defined using the standard deviation and mean value. Very high and high temperature areas were concentrated in the suburban areas, areas surrounding the suburbs, and in areas of open bare land; the main roads linking the city and the surrounding towns also appeared to have high or very high temperatures. Overall, the very high temperature class covered the majority of the suburbs. The area covered by each temperature class throughout the study period is shown in Table 5. The medium-temperature class covered the largest area over the five time periods, followed by the high-temperature class. Along with the decrease in the amount of green space, the area corresponding to the very low-temperature class also gradually decreased. In contrast, as a result of the built-up area expansion, the areas covered by the medium- and high-temperature classes increased considerably. The area of high and very high LST increased from 18,304.38 km^2 in 2000 to 23,240.70 km^2 in 2020 in the study

area. Population growth, industrial development, the large number of vehicles, and traffic congestion are also connected to the increase in the areas denoted as being medium- and high-temperature classes [57,58].

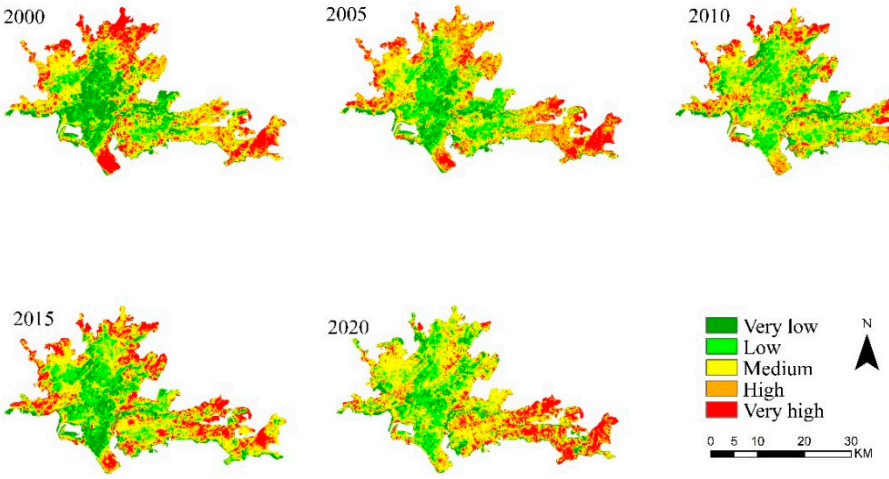

Figure 5. NLST classification map in 2000, 2005, 2010, 2015, and 2020.

Table 5. Area covered by each NLST class (km^2).

Temperature Class	Very Low Temperature	Low Temperature	Medium Temperature	High Temperature	Very High Temperature
Range	(T ≤ Tmean − 1STD)	(Tmean − 1STD < T <Tmean − 0.5STD)	(Tmean − 0.5STD < T <Tmean + 0.5STD)	(Tmean + 0.5STD < T <Tmean + 1STD)	(Tmean + 1STD < T)
Year					
2000	15,687.36	10,872.99	27,408.42	3675.51	14,628.87
2005	11,025.90	14,597.91	27,034.11	17,903.16	10,696.77
2010	8844.30	17,358.57	31,042.08	13,228.56	10,783.26
2015	11,649.96	18,408.15	26,046.63	12,450.24	12,702.69
2020	9451.89	14,931.09	33,634.26	10,318.41	12,922.29

4.2.2. Variations in the Surface Urban Heat Island Intensity

The acquired satellite imagery was used to assess the spatiotemporal variations of SUHI over Karachi during the study period (2000–2020). The results showed that the SUHI intensity increased over this period due to the continual expansion of the built-up area. The areas corresponding to a very high, high, or moderate SUHII increased, whereas those in which the SUHII was classified as low or having no SUHI decreased to a certain extent (Table 6).

Table 6. Spatiotemporal variations in the area covered by different SUHII zones (hectares).

SUHI Zone	2000	2005	2010	2015	2020
None/No SUHI	0.43	0.02	0.27	0.63	0.09
Low	0.67	0.76	1.31	1.3	1.13
Moderate	0.55	0.87	0.88	0.94	1.39
High	0.29	0.56	0.44	0.57	0.96
Very High	0.21	0.31	0.09	0	0.33

Figure 6 displays the spatial patterns of SUHII for different years during the study period. In 2000, the SUHII was very low in most of Karachi's core areas; however, there were small pockets of moderate and high SUHII in the northwest, north, and south of the city. In the outskirts of Karachi, the situation was different. Very high SUHI zones increased from 0.21 hectares in 2000 to 0.33 hectares in 2020. Similarly, high and moderate zones increased from 0.29 and 0.55 hectares in 2000 to 0.95 and 01.39 hectares in 2020. These areas

experienced haphazard expansion of the built-up areas during the study period and also included areas of exposed barren rocky outcrops that formed ridges and low hills. The exposed rocks with little vegetation coverage received direct solar radiation, which was converted into heat energy, resulting in a high LST. These factors resulted in a SUHI that was more intense than in the urban core [59].

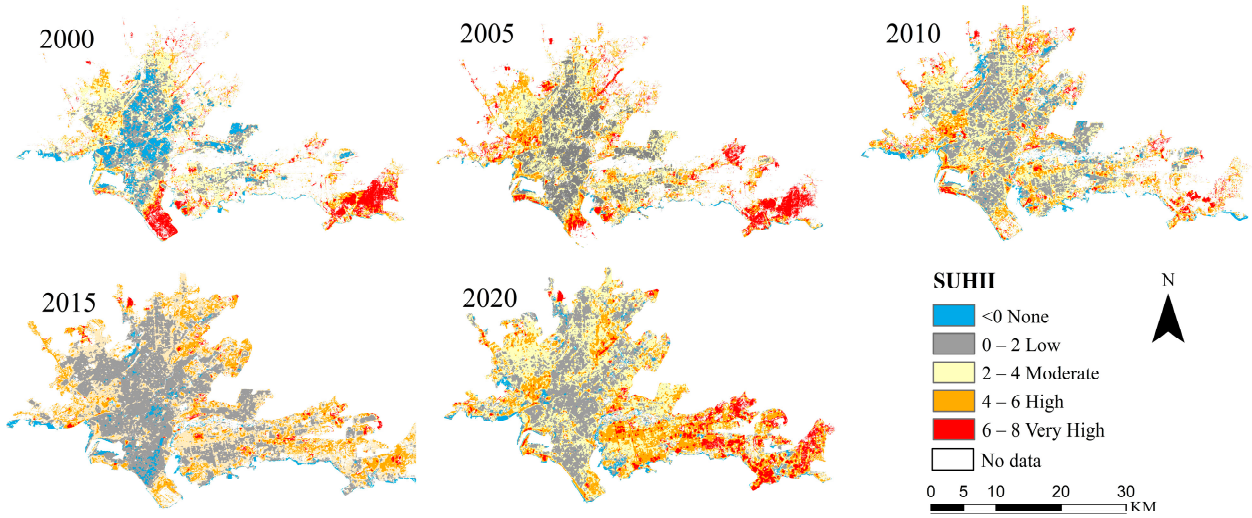

Figure 6. Spatial patterns in the SUHII (°C) in the study area for five different years during the period 2000–2020.

4.3. Relationship between Variations of LST and Land Cover Changes

4.3.1. Relationship between Land Cover Types and Land Surface Temperature

The relationships between the NLST and the four land cover categories used in this study are illustrated in Figure 7. The increase in the NLST with time reflects the increase in the size and intensity of the urban heat island because of the land use/land cover changes and the built-up area expansion in the study area [41]. These trends have become more pronounced since 2000, as, after this date, the areas surrounding Karachi that were formerly agricultural and open bare land ceased to be cultivated and became built-up areas. Significant variations between the average NLST of the different land cover classes can be seen. For the vegetation and water body classes, a relatively large range of temperatures was observed over the study period. Changes in the vegetation density within the metropolitan area may be responsible for the LST variation for this class. Many investigators observed a negative relationship between the amount of vegetation and the land surface temperature [11,28]. As a result of the inclusion of mixed pixels, the land surface temperatures of the water bodies can be influenced by the temperature of the surroundings, for example, bare land. This may be a reason for the high NLST values observed in pixels that represent water bodies. It was observed that land cover types that were converted into built-up and open bare land classes were those for which the temperature increase was the greatest.

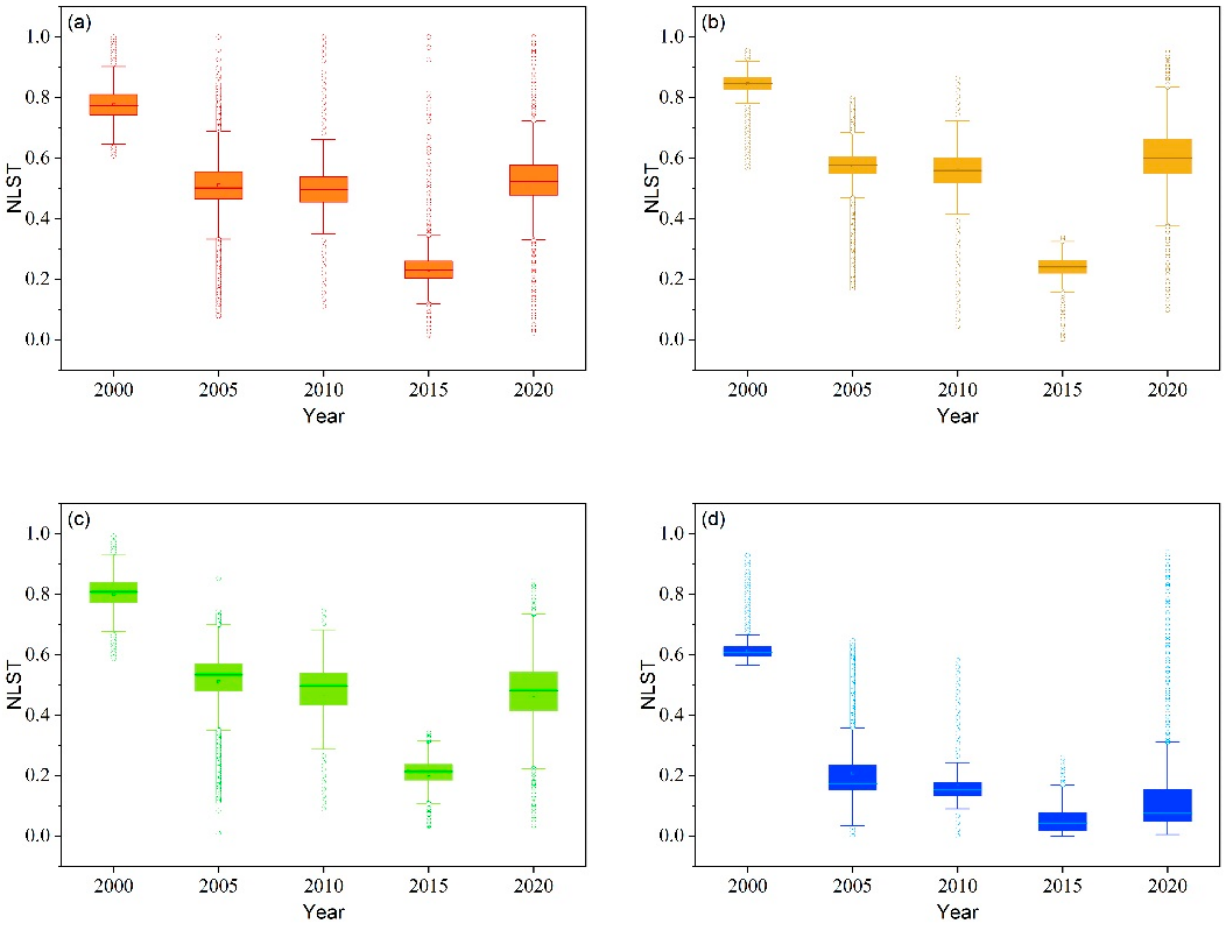

Figure 7. Box plots of normalized land surface temperatures for different land cover types: (**a**) built-up area, (**b**) bare land, (**c**) vegetation, and (**d**) water bodies.

4.3.2. Relationship between Land Cover Composition and Normalized Land Surface Temperature

The NDVI and NDBI maps of Karachi for 2000 and 2020 are shown in Figure 8a,b, respectively. The NDVI values varied from −0.17 to 0.46 in 2000 and from −0.12 to 0.45 in 2020. In 2000 and 2020, high NDVI values were observed in the eastern part of the study area, which was covered by cultivated land. In 2000, the NDBI values were in the range of −0.40 to 0.36; in 2020, they were between −0.36 and 0.55. In 2000, areas with high NDBI values were mainly concentrated in the central and the northwest of the Malir River. By 2020, the area with high NDBI values had increased and also expanded to the southern and northeastern sides of the river (Figure 8b). These spatial patterns in the NDBI are consistent with the observed patterns in urban land use changes (Figure 3) and the NLST (Figure 6) in the study area.

The calculated Pearson's correlation coefficient values indicated a significant positive correlation among the NLST and NDBI for all the land cover types throughout the study area (Figure 9). The built-up area exhibited the strongest correlation between the NDBI and NLST; the correlation was weakest for the areas covered by water bodies (0.012 in 2000 and 0.0026 in 2020). There was a weak correlation between the NLST with NDVI for all land cover types. This correlation was strongest for the vegetation class (0.319 in 2000 and 0.183 in 2020). The built-up and bare land categories exhibited the lowest correlation coefficients (0.029 and 0.177, respectively, in 2000 and 0.001 and 0.010, respectively, in 2020). The relationship between the NLST and NDVI demonstrated that the higher the vegetation density within a region, the lower the land surface temperature detected.

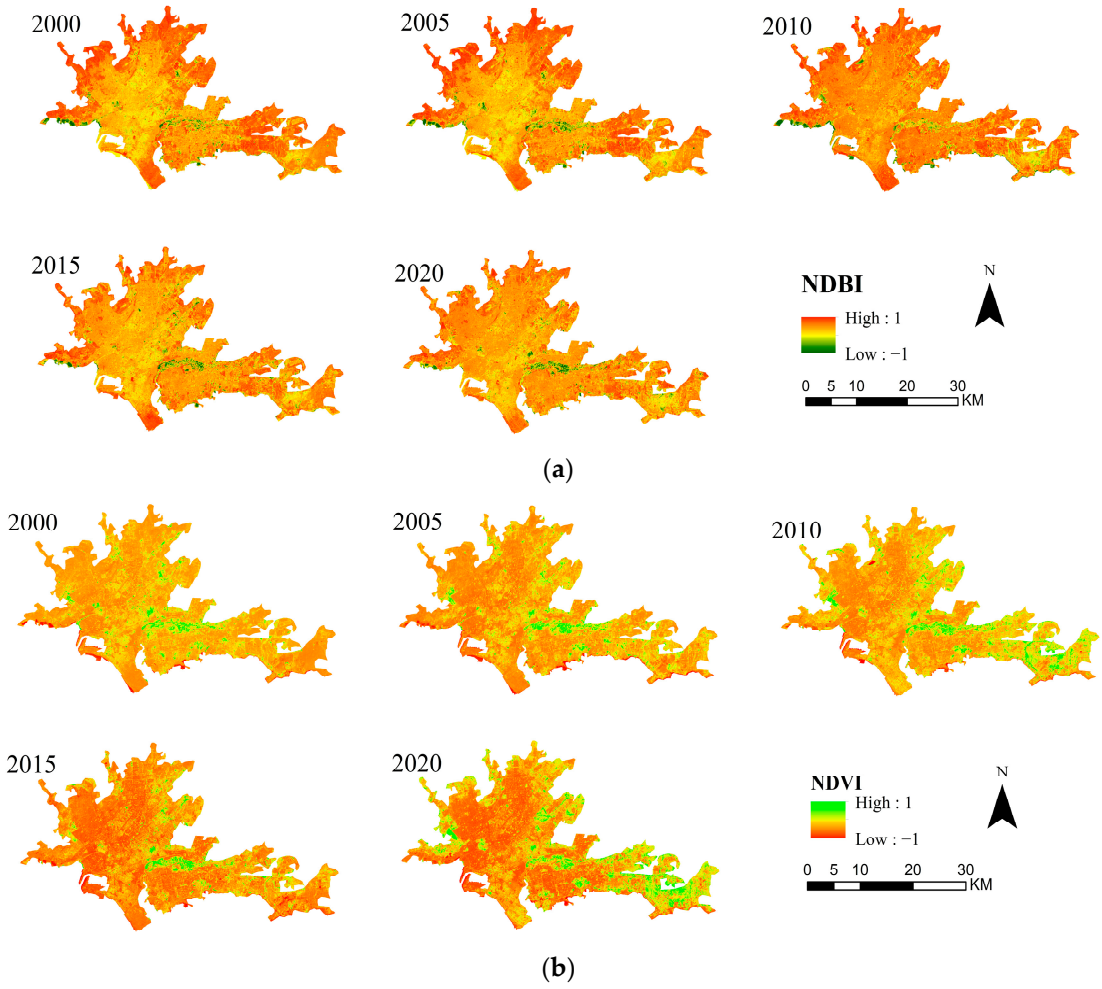

Figure 8. Maps of the (**a**) NDBI and (**b**) NDVI for Karachi for 2000, 2005, 2010, 2015, and 2020.

Figure 10 shows the distributions of the correlation coefficients for these two relationships, together with the corresponding values of the local adjusted R^2. The GWR analysis captured the spatial variation of the relationships between the NDVI and NDBI and the NLST. There was considerable spatial variation in the GWR results for different land cover classes. In the east and northeast of the study area, there was a strong positive correlation between the NLST and the NDBI, with coefficient values ranging from 0.82 to 0.88 in the urban core (Figure 10a). These areas mainly consisted of high-density urban residential and commercial areas and included the districts of Central, East, Korangi, and Kiamari. The CBD of Karachi is almost entirely built-up with sparsely distributed small-sized green spaces. The correlation between the NLST and the urban density was very low in these areas. The areas in which the correlation between the NLST and the NDVI was strongly negative were situated in the northern, eastern, and western parts of the study area (Figure 10c). These areas included large parks that have grasslands with dense vegetation. The relationship between the NDVI and NLST was very weak near to the coast. This may be due to the large uncertainty in the NDVI estimates that resulted from the presence of mixed pixels that included both water and vegetation. These uncertainties can be minimized by using remote sensing data from sensors with higher spatial resolution, such as Sentinel and Gaofen satellites [60–62]. Figure 10b,d demonstrate the GWR model's overall fitness: a high adjusted R^2 value indicates good model fitness.

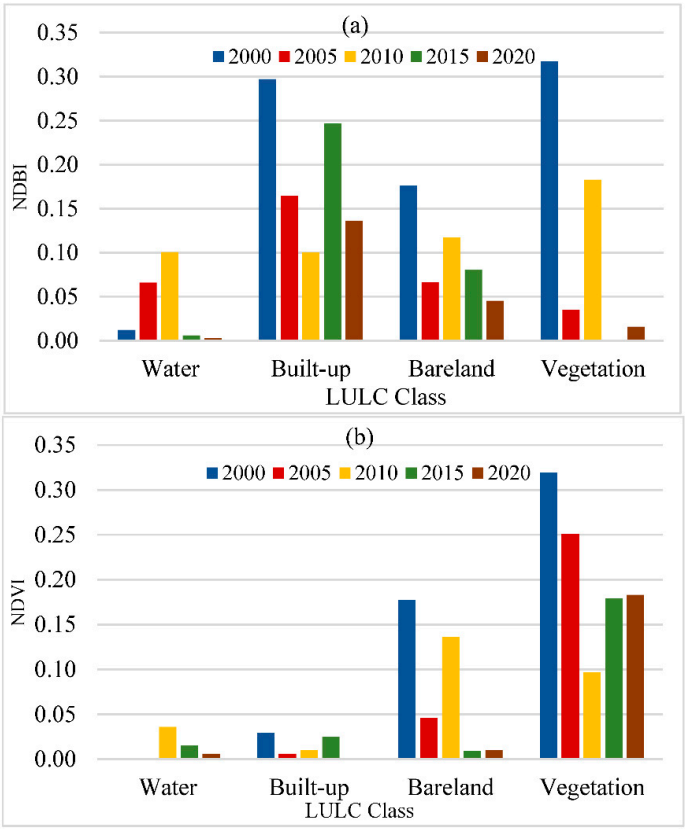

Figure 9. Relationship between the NLST and (**a**) NDVI and (**b**) NDBI, as given by the Pearson's correlation coefficient value.

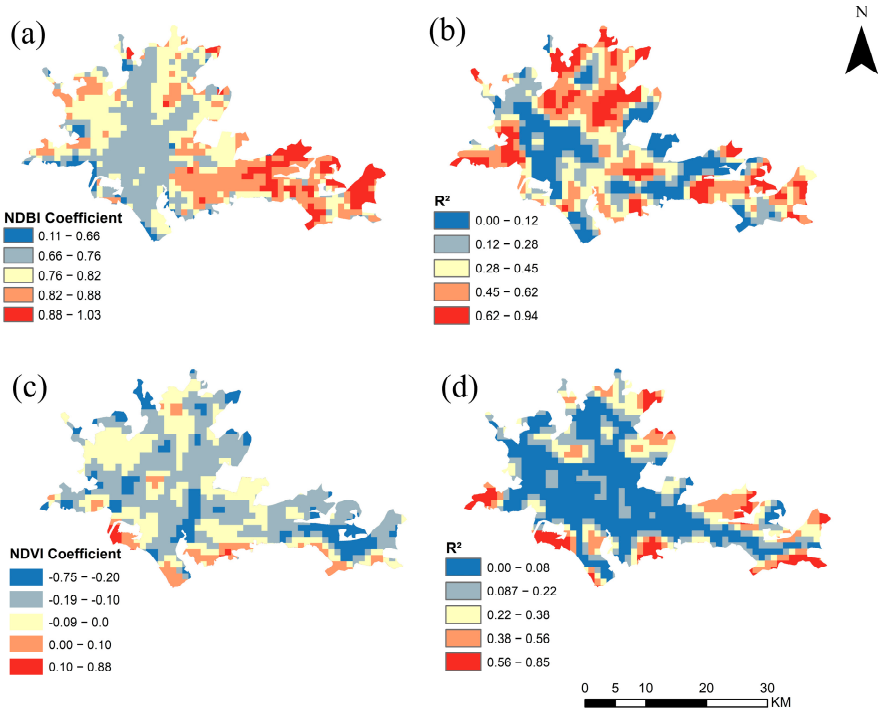

Figure 10. Results of the GWR analysis: correlation coefficients between the NLST and (**a**) the NDBI and (**b**) the corresponding local R^2 and correlation coefficients between the NLST and (**c**) the NDVI and (**d**) the corresponding local R^2.

5. Discussion

In this study, we describe the rapid expansion in the built-up area of Karachi during the period from 2000 to 2020. It was shown that this expansion primarily occurred at the expense of areas that were previously planted with crops or were open bare land. Expansion of built-up areas at the expense of cropland during the process of urbanization has also been noted in other Pakistani metropolises, including Lahore [63], Peshawar [64], and Islamabad [65]. An important feature observed concerning LULC changes in Karachi during 2000–2020 was that the cropland and open bare land were first converted into areas of open land before becoming part of the built-up area. This type of change pattern was also observed in high-density metropolitan cities, such as Hyderabad [33] and Faisalabad [66]. This process was due to the fact that agricultural land and other types of land acquired by real estate companies were left open for many years before being rebuilt or restructured.

As compared to impervious surface types, such as roads, buildings, and industrial areas, the evapotranspiration in the vegetated areas is greater. In these areas, the vegetation canopy also provides shading, and as a result, the temperature is lower [67]. The rising trend in NLST across all land cover types implies an overall surface warming trend. Although the SUHII fluctuated, the proportion of areas in which the SUHII was classified as high increased in almost all subdistricts. The SUHII increased to the greatest extent in the subdivisions with the lowest vegetation cover. In these areas, shrubland and grassland were converted into high-density built-up areas. This is in accordance with the results of previous studies in which it was shown that the core areas of cities experience the greatest increase in SUHII due to the dense nature of the built-up area and the high population density [68]. In contrast, our study demonstrates that the SUHII increased more in the peripheral areas of Karachi, such as Korangi, Landhi, Ibrahim Hyderi, Bin Qasim, Shah Faisal, and Model Colony, than in the central areas. The greater rise in the SUHII in the countryside areas may be linked to the large-scale conversion of cropland and open bare land to built-up areas. The government encourages new housing schemes and the migration of people from central areas to suburban and rural areas. The new housing schemes increase the funding of public infrastructures, educational institutes, and transportation networks to CBD areas. However, the SUHII in these areas is exacerbated by the rapid construction of the new settlements and other public infrastructures.

The regression analysis results presented in this study suggest that the GWR model can produce good results and provide detailed information at the local scale. According to the adjusted R^2 values, the GWR model can explain 84% of the variation in the land surface temperature in the study area [69,70]. From north to south, there was a trend from a negative correlation to a positive NDVI correlation, with the values of the adjusted NDVI R^2 ranging from −3.159 to 4.195. According to the land cover classification results, the built-up area density in the southern part of the city core was low. To the north of the core area, the vegetation density was high and stable, and the variations of the NDVI were observed to have a significant impact on the LST. This can be attributed to the strong cooling effect that vegetation produces in these areas. This study found that aggregated green space in parks was more effective in terms of providing cooling effects than scattered vegetation patches in the urban core. Increasing the total area and aggregation level of green space can considerably alleviate the negative impact of urban heat islands. Furthermore, in Pakistan, geospatial data are not freely shared due to various institutional and technical problems [71,72]. The openness of geospatial data collected by different government departments can facilitate the understanding of the relationship between urbanization and UHI.

Although this study provides a comprehensive description of SUHI variability, further work is necessary to investigate the influence of the spatial patterns in LULC on the SUHII, as this remains unclear. This can be achieved by applying high-resolution remote sensing data and multiscale landscape pattern analysis approaches [41,73]. Moreover, a time series analysis could provide a more precise picture of the SUHI variation in Karachi in relation to LULC changes. The findings of this study are restricted to one coastal city in Pakistan.

The association between LST and land cover may vary in different cities. Therefore, to fully grasp the impacts of urban land cover characteristics on the LST, the relationship between LULC and the LST should be examined by comparing cities in different settings [74].

6. Conclusions

The analysis of LULC change and its influence on the SUHII and the urban thermal environment of Karachi performed in this study demonstrated that the SUHII grew exponentially in Karachi during the period from 2000 to 2020. The size of the built-up area increased massively, whereas the amount of open bare land declined by more than 76.76% during this period, and the area covered by vegetation increased by 68.35%. These changes significantly altered the patterns of SUHII within Karachi, Pakistan. During the study period, the areas in which the SUHII intensity was classified as moderate, high, and very high increased from 0.55% to 1.39%, 0.29% to 0.96%, and 0.21% to 0.33% of the study area, respectively. It was also found that the SUHII increased to the greatest extent in the peripheral subdivisions in the eastern and northern parts of the city, in which there was the greatest expansion in the urban area at the expense of areas of vegetation and open bare land.

The GWR technique was used in this study. The highest NDBI regression coefficients were found in the districts situated in the east and the west, including Kamari and Malir. The southern and central parts of the city were found to have the lowest NDBI coefficients. This information could aid decision-makers in developing policies at the regional scale and fine-tuning planning practices at the local scale, with the aim of improving thermal conditions and promoting sustainable development in less-developed regions. From the regression coefficient map, the areas in which green space was most effective in terms of mitigating UHI effects were identified. Large- and medium-sized parks with dense and aggregated vegetation coverage are recommended in order to improve the thermal environment in Karachi. Moreover, future land use and land cover changes can be modeled to help decision-makers enhance the thermal resilience in cities under different land change conditions more effectively.

Author Contributions: Conceptualization, L.L. and F.C.; methodology, M.F.B., L.P. and S.N.-u.-H.; formal analysis, M.F.B., L.P. and B.L.; writing—original draft preparation, L.L. and M.F.B.; writing—review and editing, L.L., M.F.B., F.C., S.Q., S.N.-u.-H., A.T. and Q.L.; and funding acquisition, L.L. All authors have read and agreed to the published version of the manuscript.

Funding: This work was supported by the Strategic Priority Research Program of the Chinese Academy of Sciences (grant number XDA19030502) and the National Natural Science Foundation of China (grant number 42071321).

Data Availability Statement: The data presented in this study are available on request from the corresponding author.

Acknowledgments: The authors are grateful for the comments from the anonymous reviewers and the editors.

Conflicts of Interest: The authors declare no conflict of interest.

References

1. Angel, S.; Parent, J.; Civco, D.L.; Blei, A.; Potere, D. The dimensions of global urban expansion: Estimates and projections for all countries, 2000–2050. *Prog. Plan.* **2011**, *75*, 53–107. [CrossRef]
2. Department of Economic and Social Affairs. *World Urbanization Prospects: The 2018 Revision*; Department of Economic and Social Affairs, UN: New York, NY, USA, 2019.
3. Zhou, M.; Lu, L.; Guo, H.; Weng, Q.; Cao, S.; Zhang, S.; Li, Q. Urban Sprawl and Changes in Land-Use Efficiency in the Beijing–Tianjin–Hebei Region, China from 2000 to 2020: A Spatiotemporal Analysis Using Earth Observation Data. *Remote Sens.* **2021**, *13*, 2850. [CrossRef]
4. Oke, T.R.; Stewart, I.D. Local Climate Zones for Urban Temperature Studies. *Bull. Am. Meteorol. Soc.* **2012**, *93*, 1879–1900. [CrossRef]

5. Lu, L.; Weng, Q.; Guo, H.; Feng, S.; Li, Q. Assessment of urban environmental change using multi-source remote sensing time series (2000–2016): A comparative analysis in selected megacities in Eurasia. *Sci. Total Environ.* **2019**, *684*, 567–577. [CrossRef]
6. Sobrino, J.A.; Oltra-Carrió, R.; Sòria, G.; Jiménez-Muñoz, J.C.; Franch, B.; Hidalgo, V.; Mattar, C.; Julien, Y.; Cuenca, J.; Romaguera, M.; et al. Evaluation of the surface urban heat island effect in the city of Madrid by thermal remote sensing. *Int. J. Remote Sens.* **2013**, *34*, 3177–3192. [CrossRef]
7. Grimmond, S. Urbanization and Global Environmental Change: Local Effects of Urban Warming. *Geogr. J.* **2007**, *173*, 83–88. Available online: https://www.jstor.org/stable/30113496 (accessed on 15 July 2021). [CrossRef]
8. Kikegawa, Y.; Genchi, Y.; Yoshikado, H.; Kondo, H. Development of a numerical simulation system toward comprehensive assessments of urban warming countermeasures including their impacts upon the urban buildings' energy-demands. *Appl. Energy* **2003**, *76*, 449–466. [CrossRef]
9. Lu, L.; Guo, H.; Corbane, C.; Li, Q. Urban sprawl in provincial capital cities in China: Evidence from multi-temporal urban land products using Landsat data. *Sci. Bull.* **2019**, *64*, 955–957. [CrossRef]
10. Güneralp, B.; Lwasa, S.; Masundire, H.; Parnell, S.; Seto, K.C. Urbanization in Africa: Challenges and opportunities for conservation. *Environ. Res. Lett.* **2017**, *13*, 015002. [CrossRef]
11. Hassan, T.; Zhang, J.; Prodhan, F.A.; Pangali Sharma, T.P.; Bashir, B. Surface Urban Heat Islands Dynamics in Response to LULC and Vegetation across South Asia (2000–2019). *Remote Sens.* **2021**, *13*, 3177. [CrossRef]
12. Kikon, N.; Singh, P.; Singh, S.K.; Vyas, A. Assessment of urban heat islands (UHI) of Noida City, India using multi-temporal satellite data. *Sustain. Cities Soc.* **2016**, *22*, 19–28. [CrossRef]
13. Arshad, S.; Ahmad, S.R.; Abbas, S.; Asharf, A.; Siddiqui, N.A.; Islam, Z.U. Quantifying the contribution of diminishing green spaces and urban sprawl to urban heat island effect in a rapidly urbanizing metropolitan city of Pakistan. *Land Use Policy* **2022**, *113*, 105874. [CrossRef]
14. Waseem, S.; Khayyam, U. Loss of vegetative cover and increased land surface temperature: A case study of Islamabad, Pakistan. *J. Clean. Prod.* **2019**, *234*, 972–983. [CrossRef]
15. Cai, D.; Fraedrich, K.; Guan, Y.; Guo, S.; Zhang, C. Urbanization and the thermal environment of Chinese and US-American cities. *Sci. Total Environ.* **2017**, *589*, 200–211. [CrossRef]
16. Peng, J.; Jia, J.; Liu, Y.; Li, H.; Wu, J. Seasonal contrast of the dominant factors for spatial distribution of land surface temperature in urban areas. *Remote Sens. Environ.* **2018**, *215*, 255–267. [CrossRef]
17. Li, J.; Song, C.; Cao, L.; Zhu, F.; Meng, X.; Wu, J. Impacts of landscape structure on surface urban heat islands: A case study of Shanghai, China. *Remote Sens. Environ.* **2011**, *115*, 3249–3263. [CrossRef]
18. Liu, L.; Zhang, Y. Urban heat island analysis using the Landsat TM data and ASTER data: A case study in Hong Kong. *Remote Sens.* **2011**, *3*, 1535–1552. [CrossRef]
19. Zhou, D.; Bonafoni, S.; Zhang, L.; Wang, R. Remote sensing of the urban heat island effect in a highly populated urban agglomeration area in East China. *Sci. Total Environ.* **2018**, *628*, 415–429. [CrossRef]
20. Choi, Y.-Y.; Suh, M.-S.; Park, K.-H. Assessment of surface urban heat islands over three megacities in East Asia using land surface temperature data retrieved from COMS. *Remote Sens.* **2014**, *6*, 5852–5867. [CrossRef]
21. Maharjan, M.; Aryal, A.; Man Shakya, B.; Talchabhadel, R.; Thapa, B.R.; Kumar, S. Evaluation of Urban Heat Island (UHI) Using Satellite Images in Densely Populated Cities of South Asia. *Earth* **2021**, *2*, 86–110. [CrossRef]
22. Tran, H.; Uchihama, D.; Ochi, S.; Yasuoka, Y. Assessment with satellite data of the urban heat island effects in Asian mega cities. *Int. J. Appl. Earth Obs. Geoinf.* **2006**, *8*, 34–48. [CrossRef]
23. Lee, K.; Kim, Y.; Sung, H.C.; Ryu, J.; Jeon, S.W. Trend analysis of urban heat island intensity according to urban area change in Asian mega cities. *Sustainability* **2020**, *12*, 112. [CrossRef]
24. Petropoulos, G.; Ireland, G.; Griffiths, H.; Islam, T.; Kalivas, D.; Anagnostopoulos, V.; Hodges, C.; Srivastava, P. Spatiotemporal estimates of surface Soil Moisture from space using the Ts/VI feature space. In *Satellite Soil Moisture Retrieval*; Elsevier: Amsterdam, The Netherlands, 2016; pp. 91–108.
25. Guha, S.; Govil, H.; Dey, A.; Gill, N. Analytical study of land surface temperature with NDVI and NDBI using Landsat 8 OLI and TIRS data in Florence and Naples city, Italy. *Eur. J. Remote Sens.* **2018**, *51*, 667–678. [CrossRef]
26. Chen, X.-L.; Zhao, H.-M.; Li, P.-X.; Yin, Z.-Y. Remote sensing image-based analysis of the relationship between urban heat island and land use/cover changes. *Remote Sens. Environ.* **2006**, *104*, 133–146. [CrossRef]
27. Zhou, G.; Wang, H.; Chen, W.; Zhang, G.; Luo, Q.; Jia, B. Impacts of Urban land surface temperature on tract landscape pattern, physical and social variables. *Int. J. Remote Sens.* **2020**, *41*, 683–703. [CrossRef]
28. Rizvi, S.H.; Fatima, H.; Iqbal, M.J.; Alam, K. The effect of urbanization on the intensification of SUHIs: Analysis by LULC on Karachi. *J. Atmos. Sol.-Terr. Phys.* **2020**, *207*, 105374. [CrossRef]
29. Ranagalage, M.; Morimoto, T.; Simwanda, M.; Murayama, Y. Spatial analysis of urbanization patterns in four rapidly growing south Asian cities using Sentinel-2 Data. *Remote Sens.* **2021**, *13*, 1531. [CrossRef]
30. Salim, A.; Ahmed, A.; Ashraf, N.; Ashar, M. Deadly Heat Wave in Karachi, July 2015: Negligence or Mismanagement? *Int. J. Occup. Environ. Med.* **2015**, *6*, 249. [CrossRef]
31. Rahman, A.; Abdullah, H.M.; Tanzir, M.T.; Hossain, M.J.; Khan, B.M.; Miah, M.G.; Islam, I. Performance of different machine learning algorithms on satellite image classification in rural and urban setup. *Remote Sens. Appl. Soc. Environ.* **2020**, *20*, 100410. [CrossRef]

32. Hassan, Z.; Shabbir, R.; Ahmad, S.S.; Malik, A.H.; Aziz, N.; Butt, A.; Erum, S. Dynamics of land use and land cover change (LULCC) using geospatial techniques: A case study of Islamabad Pakistan. *SpringerPlus* **2016**, *5*, 812. [CrossRef]
33. Ul Din, S.; Mak, H.W.L. Retrieval of Land-Use/Land Cover Change (LUCC) Maps and Urban Expansion Dynamics of Hyderabad, Pakistan via Landsat Datasets and Support Vector Machine Framework. *Remote Sens.* **2021**, *13*, 3337. [CrossRef]
34. Pakistan Bureau of Statistics. Government of Pakistan. 2017. Available online: https://www.pbs.gov.pk/content/final-results-census-2017 (accessed on 31 July 2021).
35. Bremner, J.; Frost, A.; Haub, C.; Mather, M.; Ringheim, K.; Zuehlke, E. World population highlights: Key findings from PRB's 2010 world population data sheet. *Popul. Bull.* **2010**, *65*, 1–12.
36. Baqa, M.F.; Chen, F.; Lu, L.; Qureshi, S.; Tariq, A.; Wang, S.; Jing, L.; Hamza, S.; Li, Q. Monitoring and Modeling the Patterns and Trends of Urban Growth Using Urban Sprawl Matrix and CA-Markov Model: A Case Study of Karachi, Pakistan. *Land* **2021**, *10*, 700. [CrossRef]
37. Neteler, M. Estimating daily land surface temperatures in mountainous environments by reconstructed MODIS LST data. *Remote Sens.* **2010**, *2*, 333–351. [CrossRef]
38. Shaikh, A.A.; Gotoh, K. A satellite remote sensing evaluation of urban land cover changes and its associated impacts on water resources in Karachi, Pakistan. *NED Univ. J. Res.* **2008**, *5*, 41–56. [CrossRef]
39. Tomlinson, C.J.; Chapman, L.; Thornes, J.E.; Baker, C. Remote sensing land surface temperature for meteorology and climatology: A review. *Meteorol. Appl.* **2011**, *18*, 296–306. [CrossRef]
40. Shih, H.-c.; Stow, D.A.; Tsai, Y.H. Guidance on and comparison of machine learning classifiers for Landsat-based land cover and land use mapping. *Int. J. Remote Sens.* **2019**, *40*, 1248–1274. [CrossRef]
41. Lu, L.; Weng, Q.; Xiao, D.; Guo, H.; Li, Q.; Hui, W. Spatiotemporal Variation of Surface Urban Heat Islands in Relation to Land Cover Composition and Configuration: A Multi-Scale Case Study of Xi'an, China. *Remote Sens.* **2020**, *12*, 2713. [CrossRef]
42. Firozjaei, M.K.; Kiavarz, M.; Alavipanah, S.K.; Lakes, T.; Qureshi, S. Monitoring and forecasting heat island intensity through multi-temporal image analysis and cellular automata-Markov chain modelling: A case of Babol city, Iran. *Ecol. Indic.* **2018**, *91*, 155–170. [CrossRef]
43. Bechtel, B.; Demuzere, M.; Mills, G.; Zhan, W.; Sismanidis, P.; Small, C.; Voogt, J. SUHI analysis using Local Climate Zones—A comparison of 50 cities. *Urban Clim.* **2019**, *28*, 100451. [CrossRef]
44. Estoque, R.C.; Murayama, Y. Monitoring surface urban heat island formation in a tropical mountain city using Landsat data (1987–2015). *ISPRS J. Photogramm. Remote Sens.* **2017**, *133*, 18–29. [CrossRef]
45. Deilami, K.; Kamruzzaman, M.; Liu, Y. Urban heat island effect: A systematic review of spatio-temporal factors, data, methods, and mitigation measures. *Int. J. Appl. Earth Obs. Geoinf.* **2018**, *67*, 30–42. [CrossRef]
46. Buyantuyev, A.; Wu, J. Urban heat islands and landscape heterogeneity: Linking spatiotemporal variations in surface temperatures to land-cover and socioeconomic patterns. *Landsc. Ecol.* **2010**, *25*, 17–33. [CrossRef]
47. Siqi, J.; Yuhong, W. Effects of land use and land cover pattern on urban temperature variations: A case study in Hong Kong. *Urban Clim.* **2020**, *34*, 100693. [CrossRef]
48. Chen, T.-L.; Lin, Z.-H. Impact of land use types on the spatial heterogeneity of extreme heat environments in a metropolitan area. *Sustain. Cities Soc.* **2021**, *72*, 103005. [CrossRef]
49. Hamza, S.; Khan, I.; Lu, L.; Liu, H.; Burke, F.; Nawaz-ul-Huda, S.; Baqa, M.F.; Tariq, A. The Relationship between Neighborhood Characteristics and Homicide in Karachi, Pakistan. *Sustainability* **2021**, *13*, 5520. [CrossRef]
50. Yang, W. An Extension of Geographically Weighted Regression with Flexible Bandwidths. Ph.D. Thesis, University of St Andrews, St Andrews, UK, 2014.
51. Arif, M.; Hussain, I.; Hussain, J.; Sharma, M.K.; Kumar, S.; Bhati, G. GIS-based inverse distance weighting spatial interpolation technique for fluoride distribution in south west part of Nagaur district, Rajasthan. *Cogent Environ. Sci.* **2015**, *1*, 1038944. [CrossRef]
52. Mak, H.W.; Ng, D.C. Spatial and Socio-Classification of Traffic Pollutant Emissions and Associated Mortality Rates in High-Density Hong Kong via Improved Data Analytic Approaches. *Int. J. Environ. Res. Public Health* **2021**, *18*, 6532. [CrossRef]
53. Ke, W.; Cheng, H.P.; Yan, D.; Lin, C. The Application of Cluster Analysis and Inverse Distance-Weighted Interpolation to Appraising the Water Quality of Three Forks Lake. *Procedia Environ. Sci.* **2011**, *10*, 2511–2517. [CrossRef]
54. Szymanowski, M.; Kryza, M. Local regression models for spatial interpolation of urban heat island—an example from Wrocław, SW Poland. *Theor. Appl. Climatol.* **2012**, *108*, 53–71. [CrossRef]
55. Hasan, A. Land contestation in Karachi and the impact on housing and urban development. *Environ. Urban.* **2015**, *27*, 217–230. [CrossRef] [PubMed]
56. Building, K.; Regulations, T.P. Chapter 25. Historic Buildings. Sindh Building Control. In *Authority (SBCA) Department of Culture and Planning*; Government of Pakistan: Islamabad, Pakistan, 2002.
57. Mehdi, M.R.; Kim, M.; Seong, J.C.; Arsalan, M.H. Spatio-temporal patterns of road traffic noise pollution in Karachi, Pakistan. *Environ. Int.* **2011**, *37*, 97–104. [CrossRef] [PubMed]
58. Qureshi, S. The fast growing megacity Karachi as a frontier of environmental challenges: Urbanization and contemporary urbanism issues. *J. Geogr. Reg. Plan.* **2010**, *3*, 306–321. [CrossRef]
59. Pithawalla, M.B.; Martin-Kaye, P.H.A. *Geology and geography of Karachi and its neighbourhood*; University Microfilms: Ann Arbor, MI, USA, 1962.

60. Van Leeuwen, W.J.; Orr, B.J.; Marsh, S.E.; Herrmann, S.M. Multi-sensor NDVI data continuity: Uncertainties and implications for vegetation monitoring applications. *Remote Sens. Environ.* **2006**, *100*, 67–81. [CrossRef]
61. Roy, D.P.; Borak, J.S.; Devadiga, S.; Wolfe, R.E.; Zheng, M.; Descloitres, J. The MODIS Land product quality assessment approach. *Remote Sens. Environ.* **2002**, *83*, 62–76. [CrossRef]
62. Ghimire, P.; Lei, D.; Juan, N. Effect of image fusion on vegetation index quality—a comparative study from Gaofen-1, Gaofen-2, Gaofen-4, Landsat-8 OLI and MODIS Imagery. *Remote Sens.* **2020**, *12*, 1550. [CrossRef]
63. Mumtaz, F.; Tao, Y.; de Leeuw, G.; Zhao, L.; Fan, C.; Elnashar, A.; Bashir, B.; Wang, G.; Li, L.; Naeem, S.; et al. Modeling Spatio-Temporal Land Transformation and Its Associated Impacts on land Surface Temperature (LST). *Remote Sens.* **2020**, *12*, 2987. [CrossRef]
64. Ahmad, W.; Iqbal, J.; Nasir, M.J.; Ahmad, B.; Khan, M.T.; Khan, S.N.; Adnan, S. Impact of land use/land cover changes on water quality and human health in district Peshawar Pakistan. *Sci. Rep.* **2021**, *11*, 16526. [CrossRef]
65. Sadiq Khan, M.; Ullah, S.; Sun, T.; Rehman, A.U.; Chen, L. Land-Use/Land-Cover Changes and Its Contribution to Urban Heat Island: A Case Study of Islamabad, Pakistan. *Sustainability* **2020**, *12*, 3861. [CrossRef]
66. Dilawar, A.; Chen, B.; Trisurat, Y.; Tuankrua, V.; Arshad, A.; Hussain, Y.; Measho, S.; Guo, L.; Kayiranga, A.; Zhang, H.; et al. Spatiotemporal shifts in thermal climate in responses to urban cover changes: A-case analysis of major cities in Punjab, Pakistan. *Geomat. Nat. Hazards Risk* **2021**, *12*, 763–793. [CrossRef]
67. Bowler, D.E.; Buyung-Ali, L.; Knight, T.M.; Pullin, A.S. Urban greening to cool towns and cities: A systematic review of the empirical evidence. *Landsc. Urban. Plan.* **2010**, *97*, 147–155. [CrossRef]
68. Atasoy, M. Assessing the impacts of land-use/land-cover change on the development of urban heat island effects. *Environ. Dev. Sustain.* **2020**, *22*, 7547–7557. [CrossRef]
69. Alibakhshi, Z.; Ahmadi, M.; Farajzadeh Asl, M. Modeling biophysical variables and land surface temperature using the GWR model: Case study—Tehran and its satellite cities. *J. Indian Soc. Remote Sens.* **2020**, *48*, 59–70. [CrossRef]
70. Kashki, A.; Karami, M.; Zandi, R.; Roki, Z. Evaluation of the effect of geographical parameters on the formation of the land surface temperature by applying OLS and GWR, A case study Shiraz City, Iran. *Urban Clim.* **2021**, *37*, 100832. [CrossRef]
71. Khurshid, M.M.; Zakaria, N.; Rashid, A.; Kazmi, R.; Shafique, M. Diffusion of Big Open Data Policy Innovation in Government and Public Bodies in Pakistan. In Proceedings of the First International Conference, INTAP 2018, Bahawalpur, Pakistan, 23–25 October 2018; Revised Selected Papers. Springer: Berlin/Heidelberg, Germany, 2019; pp. 326–337. [CrossRef]
72. Khurshid, M.M.; Zakaria, N.; Rashid, A.; Ahmad, M.; Arfeen, M.; Faisal, H. Modeling of Open Government Data for Public Sector Organizations Using the Potential Theories and Determinants—A Systematic Review. *Informatics* **2020**, *7*, 24. [CrossRef]
73. Peng, J.; Hu, Y.; Dong, J.; Liu, Q.; Liu, Y. Quantifying spatial morphology and connectivity of urban heat islands in a megacity: A radius approach. *Sci. Total Environ.* **2020**, *714*, 136792. [CrossRef] [PubMed]
74. Koc, C.B.; Osmond, P.; Peters, A. Evaluating the cooling effects of green infrastructure: A systematic review of methods, indicators and data sources. *Sol. Energy* **2018**, *166*, 486–508. [CrossRef]